J Mol Model (2012) 18:851–858
DOI 10.1007/s00894-011-1119-z

ORIGINAL PAPER

Density functional theory studies on the inclusion complexes of cyclic decapeptide with 1-phenyl-1-propanol enantiomers

Hongge Zhao · Yanyan Zhu · Mingqiong Tong · Juan He · Chunmei Liu · Mingsheng Tang

Received: 8 October 2010 / Accepted: 5 May 2011 / Published online: 28 May 2011

Abstract Cyclic peptides are exciting novel hosts for chiral and molecular recognition. In this work, the inclusion complexes of cyclic decapeptide (**CDP**) with the 1-phenyl-1-propanol enantiomers (**E-PP**) are firstly studied using the density functional theory (DFT) B3LYP method. Our calculated results indicated that S(-)-1-phenyl-1-propanol (**S-PP**) could form a more stable inclusion complex with **CDP** than that of R(+)-1-phenyl-1-propanol (**R-PP**). The obvious differences in binding energy and thermodynamics data suggest that the cyclic decapeptide could differentiate the two enantiomers. Furthermore, molecular dynamics simulation results have supported the conclusions obtained by DFT. The current investigation shows that cyclic peptide is a desirable host molecule for chiral and molecular recognition.

Keywords Chiral recognition · Cyclic peptide · 1-phenyl-1-propanol · Inclusion complex

Introduction

Inclusion complex is the focus of current host-guest chemistry and supramolecular chemistry [1–5]. Experimental [6–8] and theoretical [9–13] investigations on this topic have been actively pursued for decades. Particularly, studies on searching the desired host molecules dominate the scene. Many examples of host molecules, such as cyclodextrins (CDs) [14–16], macrocyclic antibiotics [17, 18], proteins [19] and chiral micelles [20] are available now. The representative host molecule cyclodextrins (CDs) have received much attention because they can separate many enantiomers by forming inclusion complexes with specific guest molecules [21, 22], this characteristic has been successfully applied to many fields including solubility enhancement, drug delivery, chemical protection, separation technology, and supramolecular chemistry [23, 24]. Another reason of the popularity of CDs is that the high symmetry and rigidity of their structures facilitate the study of inclusion complexes by NMR techniques [25]. However, this lack of conformational flexibility is a limitation regarding efficiency of inclusion complex. It's difficult for the CDs molecules to adjust their geometries to fit the guest molecules in an optimal interaction mode. Notably, these conformational disadvantages of CDs are just good qualities for cyclic peptides which are polypeptide linked by amino acid residues. In recent years, cyclic peptides have been synthesized and used as anticancer, antimalarial, antibacterial drug carriers and enzyme inhibitors, where they act as host molecules to form inclusion complexes with biological molecules [26–29].

Understanding the structural details of the inclusion complexes of cyclic peptides with guest molecules may help us delineate the features that are responsible for the remarkable potency of cyclic peptides. However, knowledge of the precise interaction mechanism of cyclopeptides with enantiomers of a chiral molecule at the molecular level is still very limited [30]. Especially, conformations and structures of cyclic peptides are not yet clear experimentally. Some theoretical studies on the

Electronic supplementary material The online version of this article (doi:10.1007/s00894-011-1119-z) contains supplementary material, which is available to authorized users.

H. Zhao · Y. Zhu (✉) · M. Tong · J. He · C. Liu · M. Tang (✉)
Department of Chemistry, Zhengzhou University,
Zhengzhou, Henan Province 450001, People's Republic of China
e-mail: zhuyan@zzu.edu.cn

M. Tang
e-mail: mstang@zzu.edu.cn

structures of cyclic peptides have been performed over the past several years [31–34]. Guangju Chen and co-workers have reported the structural characteristics of an important type of cyclopeptides formed by cyclo[(-β^3-HGly)$_4$-] based on density function theory (B3LYP) [35]. Their results provide us with new insights into the formation of polypeptide. Inspired by the study of Guangju Chen and co-workers on cyclopeptide, we have performed a density functional theory (DFT) study of the interactions between cyclic peptides and enantiomers, which may have much theoretical and practical importance. In the present work, we focused on the structure of model cyclic peptide derived from glycine. The glycine, as the simplest amino acid, was used to create a cyclopeptide template. Cyclic decapeptide (assigned as **CDP**) (shown in Chart 1a), constructed with ten identical glycines, is used as a receptor that is capable of including trapping the guest molecules inside the peptide cavity possibly caused by the conformational flexibility and noncovalent interactions.

1-phenyl-1-propanol, a chiral molecule existing in a couple of enantiomers forms (assigned as **E-PP**, **E**=**R** or **S**, shown in Chart 1b), is a good candidate for constructing a simple model to study chiral discrimination. The separation of the enantiomers of 1-phenyl-1-propanol has already been carried out in the experiment [36]. However, the separation result is not desirable. In this work, **CDP** and **E-PP** are selected as host molecule and guest molecules, respectively, to investigate the conformational and structural features of **CDP/E-PP** and the interaction of **CDP** with **E-PP**.

Computational methods

The search of the energy minimum

In this paper, the selected initial structure of **CDP** is E-type backbone due to the E-type backbone of cyclopeptide is more stable than that of B-type when the number of amino acid residues is equal to or bigger than 10 [37].

The coordinate system used to define the inclusion process of **CDP** with **E-PP** is shown in Chart 2, which was adopted from a previous work [38]. Briefly, the **CDP** ring was positioned symmetrically around the Z-axis, such that all oxygen and nitrogen atoms in the glycine are in the XY plane. The **E-PP** molecule was docked into the cavity of **CDP** along with the Z-axis. Multiple initial positions were generated by movement of **E-PP** along the Z-axis. The relative position between **CDP** and **E-PP** was measured by the Z-coordinate of the labeled carbon atom of **E-PP** (shown in Chart 2). In order to find a more stable structure of **CDP/E-PP**, we calculated all of the structures of each E-PP molecule by scanning θ, circling around the Z-axis, at 20° intervals from -180° to 180° and scanning the Z-coordinate at 0.3 Å intervals with semi-empirical calculations (PM3), which can be currently applied in biochemical systems with its improved description of the interactions between non-bonded atoms, e.g., hydrogen bond and steric effects [39]. All of local energy minimum structures from potential energy surface (PES) by scan calculations were fully optimized at the B3LYP/3-21G level of theory [40, 41]. Subsequently, **CDP/E-PP** with the lowest energy obtained by B3LYP/3-21G calculations were fully optimized using the basis set of 6-31+G(d,p). Additionally, the frequency calculations for **CDP/E-PP** were also carried out to verify the optimized structures to be energy minima without any imaginary frequency.

Definition of the binding energy (BE)

In order to investigate the driving forces leading to **CDP/E-PP** between **CDP** and **E-PP**, the binding energy (BE) upon **CDP/E-PP** for the minimum energy structure is evaluated from the following equation.

$$B\mathbf{E} = \mathbf{E}[\mathrm{CDP/E-PP}] - \mathbf{E}[\mathrm{E-PP}] - \mathrm{E}[\mathrm{CDP}] \quad (1)$$

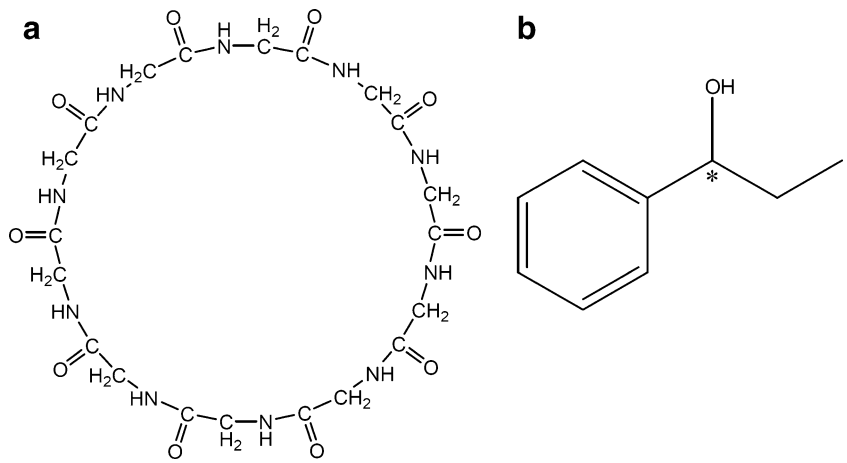

Chart 1 Schematic representation for the conformations of (**a**) cyclic decapetide (**CDP**) and (**b**) 1-phenyl-1-propanol enantiomers (**E-PP**)

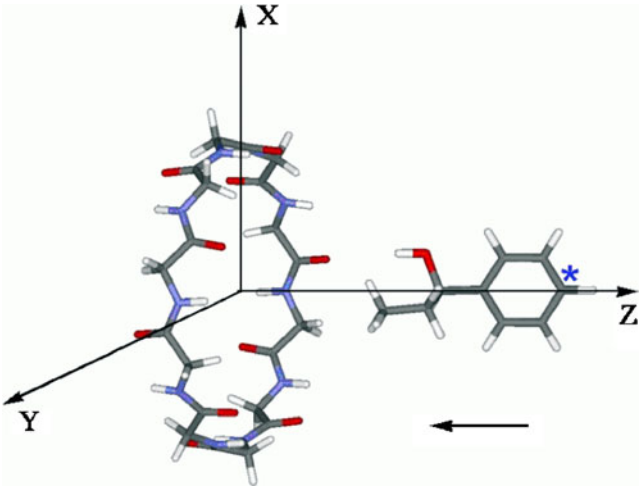

Chart 2 Coordinate systems used to define the inclusion process (H atoms included in **CDP** are omitted)

Where, **E[CDP/E-PP]**, **E[E-PP]** and **E[CDP]** represent the energies of **CDP/E-PP**, **E-PP** and **CDP**, respectively. The magnitude of BE would be a sign of the driving force toward **CDP/E-PP**. A negative value of BE means that the corresponding **CDP/E-PP** is energetically stable; the more negative the BE is, the more stable the complex is.

The deformation energies of **CDP** and **E-PP** were calculated by Eq. 2 and 3 [42].

$$\mathbf{DE}[\mathrm{E-PP}] = \mathbf{E}[\mathrm{E-PP}]_{\mathrm{sp}}^{\mathrm{opt}} - \mathbf{E}[\mathrm{E-PP}]_{\mathrm{opt}} \quad (2)$$

$$\mathbf{DE}[\mathbf{CDP}] = \mathbf{E}[\mathbf{CDP}]_{\mathrm{sp}}^{\mathrm{opt}} - \mathbf{E}[\mathbf{CDP}]_{\mathrm{opt}}, \quad (3)$$

where **DE[E-PP]** and **DE[CDP]** are the deformation energies of **E-PP** and **CDP** respectively; $\mathbf{E}[\mathrm{E-PP}]_{\mathrm{sp}}^{\mathrm{opt}}$ and $\mathbf{E}[\mathrm{E-PP}]_{\mathrm{opt}}$ are the single point energy of **E-PP** on the configuration taken from the optimized **CDP/E-PP** and the energy of the optimized geometry of **E-PP** respectively; $\mathbf{E}[\mathbf{CDP}]_{\mathrm{sp}}^{\mathrm{opt}}$ and $\mathbf{E}[\mathbf{CDP}]_{\mathrm{opt}}$ are the single point energy of **CDP** on the configuration taken from the optimized **CDP/E-PP** and the energy of the optimized geometry of **CDP** respectively.

Thermodynamic analysis for the inclusion process of CDP with E-PP

The geometries of the two inclusion complexes were fully optimized without any geometrical or symmetry constrains using the B3LYP/6-31+G(d,p) method. The frequencies were performed for the evaluation of the enthalpy changes (ΔH) and Gibbs free energy changes (ΔG) of the inclusion process between **CDP** and **E-PP**.

Moreover, the electronic properties of **CDP/E-PP** were studied using the natural bond orbital (NBO) analysis at the B3LYP/6-31+G(d,p) level of theory [43]. NBO calculations quantify the H-bond interactions between host and guest molecules via the determination of the stabilization energy $E^{(2)}$. The stabilization energy $E^{(2)}$ related to the delocalization trend of electrons from donor to acceptor orbital is calculated via perturbation theory. A large stabilization energy $E^{(2)}$ between a lone pair LP(Y) of an atom Y and an antibonding σ* (X—H) orbital is generally indicative of a strong $\mathrm{X-H\cdots Y}$ hydrogen bond [44]. Basis set superposition error (BSSE) of binding energies is calculated by using the counterpoise corrections method [45]. All calculations were carried out using the GAUSSIAN 03 program package [46].

Results and discussion

Most stable conformation and binding energy

Two obtained PESs are shown in Fig. 1. It can be seen that the inclusion processes of **CDP** with **E-PP** are energetically favorable. Interestingly, most of energy minima structures locate at approximately Z=0 Å for **E-PP** approaches. Based on the related scanned energy minima at the level of PM3, B3LYP/3-21G calculations were performed to optimize **CDP/E-PP** as presented in Fig. 2. Other possible locations and angles of **E-PP** were examined using the B3LYP method, which were shown to be energetically less favorable and therefore not listed. Based on the B3LYP/3-21G optimized equilibrium geometries of the **CDP/E-PP**, calculations at the B3LYP/6-31+G(d,p) level were then performed.

The BE values including BSSE corrections for most stable inclusion configurations are listed in Table 1. The BE values for **CDP/S-PP** and **CDP/R-PP** are -19.94 and -10.54 kJ $\mathrm{mol^{-1}}$, respectively, which demonstrate that **CDP** can form stable complexes with **E-PP**. The **CDP/S-PP** was more favorable than **CDP/R-PP** by an energy difference of 9.40 kJ $\mathrm{mol^{-1}}$, suggesting that **S-PP** is bound more firmly by **CDP**.

Energies of the inclusion complexes

To investigate the thermodynamics of the inclusion process, the statistical thermodynamic calculations were performed at the B3LYP/6-31+G(d,p) level of theory. The calculated results are listed in Table 1. It is obvious that the inclusion process of **CDP** with **E-PP** are exothermic judged from the negative enthalpy changes. The negative enthalpy changes also suggest that both the inclusion processes are enthalpically favorable. On the other hand, the enthalpy change of **CDP/S-PP** (-20.93 kJ $\mathrm{mol^{-1}}$) is about 8.30 kJ $\mathrm{mol^{-1}}$ lower than that of

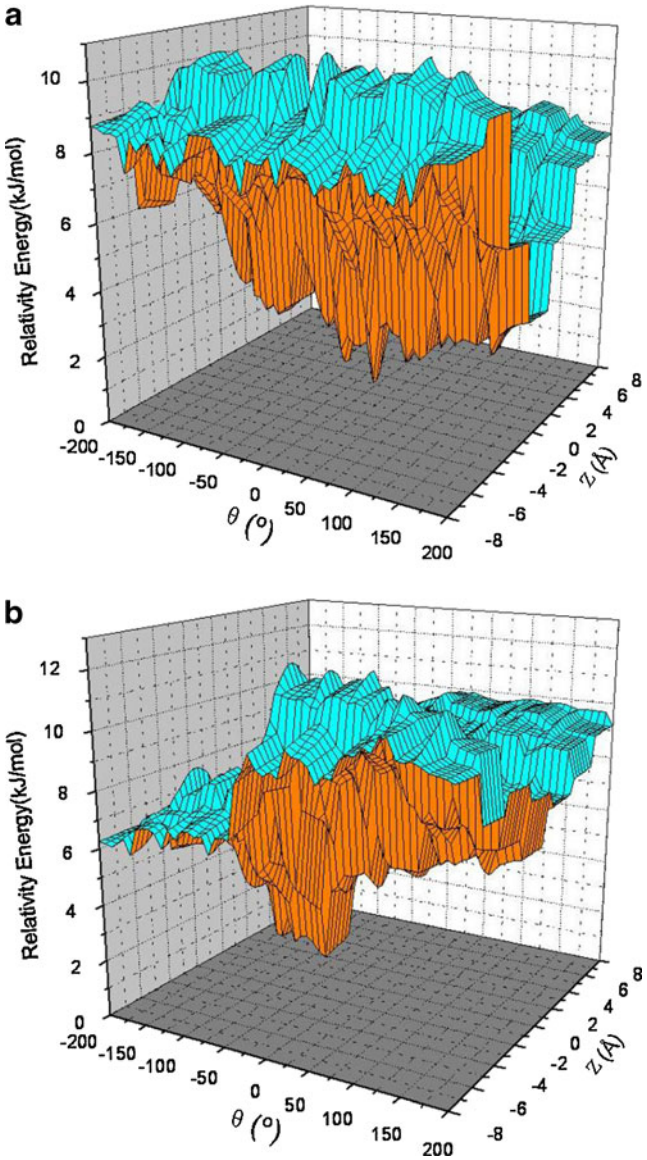

Fig. 1 Scan of total energy of the inclusion complex of the **E-PP** enantiomers into **CDP** at different positions (z) and orientations (θ): (**a**) S(-)-1-phenyl-1-propanol (**S-PP**) and **CDP**; (**b**) R(+)-1-phenyl-1-propanol (**R-PP**) and **CDP**. The position of the **E-PP** molecule was determined by the Z-coordinate of the labeled carbon atom (*) in the phenyl group. θ refers to the angle of each guest molecule circling around the Z-axis of the system

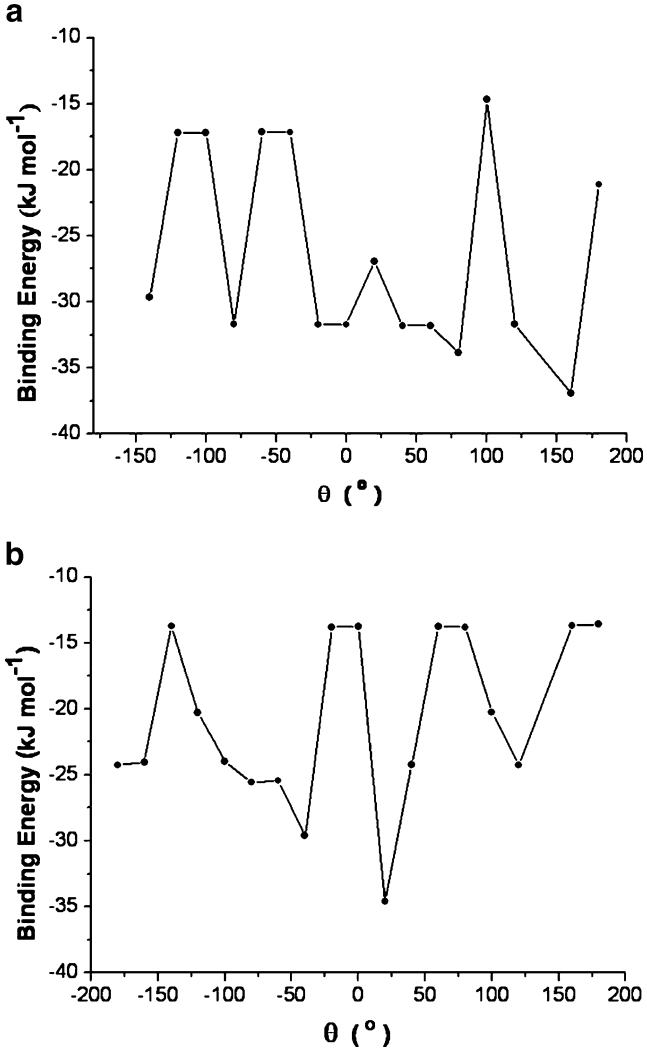

Fig. 2 B3LYP/3-21G stabilization energy including BSSE correction of the **CDP/E-PP**: (**a**) **S-PP** and **CDP**; (**b**) **R-PP** and **CDP**. θ refers the start angle of each guest molecule into **CDP** circling around the Z-axis of the system

CDP/R-PP (-12.63 kJ mol^{-1}). The thermodynamic results indicate that the **S-PP** structure is preferred to form inclusion complex with **CDP** based on enthalpy grounds.

One interesting feature of the guest is its conformational flexibility. A better guest conformational flexibility is favorable to the host–guest interactions, it makes it possible for the guest molecule to modify its conformation to ensure a better penetration [47]. Investigation of the deformation energy of the chosen guest **E-PP** at the B3LYP/6-31+G(d,p) level of theory (as shown in Table 1) demonstrated that the deformation of **S-PP** requires slightly more energy to adapt conformation to fit the cavity of **CDP** than that of **R-PP** as indicated by the **DE[E-PP]** data of about 2.29 and 0.93 kJ mol^{-1} respectively. On the other hand, there are some distortion of **CDP** in the inclusion process as well. **CDP** needs 3.68 kJ mol^{-1} to adapt conformational adaptation for **CDP/S-PP** and 1.48 kJ mol^{-1} for **CDP/R-PP**, indicating that the deformation of **CDP** is advantageous for the inclusion complex formation.

Conformational characteristics of CDP/E-PP

The favorable structures of **CDP/E-PP** optimized at the B3LYP/6-31+G(d,p) level are graphically presented in Fig. 3. Figure 3a shows that for **CDP/S-PP**, the phenyl of

Table 1 The binding energies and thermodynamic parameters upon the inclusion complexes of **CDP/S-PP** and **CDP/R-PP** at the B3LYP/6-31+G(d,p) level of theory

Parameter	CDP/S-PP	CDP/R-PP
BE[a](kJ mol^{-1})	-27.67	-18.79
BSSE(kJ mol^{-1})	7.73	8.25
BE[b](kJ mol^{-1})	-19.94	-10.54
DE[E-PP][c] (kJ mol^{-1})	2.29	0.93
DE[CDP][d] (kJ mol^{-1})	3.68	1.48
$\Delta H°$(kJ mol^{-1})	-20.93	-12.63
$\Delta G°$(kJ mol^{-1})	28.47	37.14
$\Delta S°$(J mol^{-1} K^{-1})	-165.67	-166.95
ΔH_{pcm}[e] (kJ mol^{-1})	-6.52	5.37
ΔG_{pcm}[f] (kJ mol^{-1})	-38.34	-29.42
ΔS_{pcm}[g] (J mol^{-1} K^{-1})	106.72	116.69

[a] BE is the binding energy upon complex

[b] BE is the binding energy including the basis set superposition error (BSSE) correction

[c] **DE[E-PP]** is the deformation energy of **E-PP**

[d] **DE[CDP]** is the deformation energy of **CDP**

[e] ΔH_{pcm} is the enthalpy change obtained by PCM model

[f] ΔG_{pcm} is the Gibbs free energy change obtained by PCM model

[g] ΔS_{pcm} is the entropy change obtained by PCM model

S-PP is almost totally encapsulated in the cyclic decapeptide cavity. While the OH group remains on the rim of the **CDP**, which is in favor of formation of H-bond with some groups of **CDP**. The optimized geometries reveal that there are two hydrogen bond interactions between **CDP** and **S-PP**. Figure 3b shows clearly that for the **CDP/R-PP**, the phenyl of **R-PP** are partially included in **CDP** and the orientation of OH group directed toward the inside of the **CDP** cavity, allowing the lone pair of the oxygen atom to act as an H-bond acceptor thus stabilizing the **CDP/R-PP**.

Hydrogen bond analysis and NBO analysis

To investigate the reason why geometries of **CDP/E-PP** are different, the hydrogen bond and NBO analyses are further performed at the B3LYP/6-31+G(d,p) level of theory. The detailed information of intermolecular hydrogen bond interactions for **CDP/E-PP** are listed in Table 2 and shown in Fig. 4. It can be seen from Table 2 that the distinct differences for hydrogen bond interactions occur in the different inclusion complexes. In the **CDP/S-PP** structure, there are two hydrogen bond interactions. One occurs between O1 of **CDP** and O11 of **S-PP**, a strong hydrogen bond $O11-H11\cdots O1$ ($d_{H\ldots O}=1.93$Å). The other occurs between the O11 of **S-PP** and C10 of **CDP**, a weak hydrogen bond $C10-H10\cdots O11$ ($d_{H\ldots O}=2.48$Å). In the **CDP/R-PP** structure, only one weak hydrogen bond is formed. Namely, the O5 atom of **CDP** donates a hydrogen bond ($d_{H\ldots O}=2.22$Å) to O11 of **R-PP**. Distinctly, the intermolecular hydrogen bonds play a crucial role in the stability of inclusion complexes conformational change. It was suggested that the contribution of the $O-H\cdots O$ hydrogen bond interactions to the structural stability in **CDP/S-PP** is greater than those in **CDP/R-PP**. This explains why the BE for the **CDP/S-PP** is 9.40 kJ mol^{-1} lower than that of **CDP/R-PP**.

The following NBO analyses confirm the occurrence of these intermolecular hydrogen bonds. The stabilization energies $E^{(2)}$ calculated at the B3LYP/6-31+G(d,p) level of the established H-bond in the **CDP/E-PP** are listed in Table 2. Significant interaction energies are obtained for the expected hydrogen bonds, especially for the $O-H\cdots O$ one. The interaction energy of the $O-H\cdots O$ hydrogen bond of **CDP/S-PP** is 23.24 kJ mol^{-1}, which is a conventional hydrogen bond (16–25 kJ mol^{-1} for $O-H\cdots O$ hydrogen bonds in carbohydrates) [48]. The interaction energy of the $O-H\cdots O$ hydrogen bond of the **CDP/R-PP** is 3.61 kJ mol^{-1}, which belongs to a typical weak hydrogen bond for which energies vary between 2.1 and 8.4 kJ mol^{-1} [49]. Noteworthy, one extra $C-H\cdots O$ hydrogen bond was observed for **CDP/S-PP**. Quantum mechanical calculations have been performed to determine the energetic of the $C-H\cdots O$ bonds in the complexes, which are far below values of conventional hydrogen bonding [50, 51], but appreciably above energies of van der Waals contacts. Briefly, these hydrogen bond interactions play important roles in the inclusion processes of **CDP** with **E-PP**.

Molecular dynamics simulations

Regarding the identification of the preferred inclusion modes, it would be more realistic to select a set of inclusion complex structures, besides a single optimized configuration. Inclusion phenomena are dynamic in nature; therefore the establishment of host-guest intermolecular interactions cannot be analyzed from a single structure [52]. Perhaps, other unexplored inclusion complexes can lead to different hydrogen bonding patterns. Molecular dynamics (MD) simulations could provide such a view [53]. To obtain the possible inclusion modes between **CDP** and **E-PP**, the two guests, **R-PP** and **S-PP**, were firstly docked into **CDP** by using AutoDock 4.0 program [54]. The grid map of 32×32×32 points and a grid-point spacing of 0.375 Å have been employed during the dock processes. One better-scoring representative from 1000 predication inclusion models for **CDP** with **E-PP** has been selected as an initial structure for MD simulations.

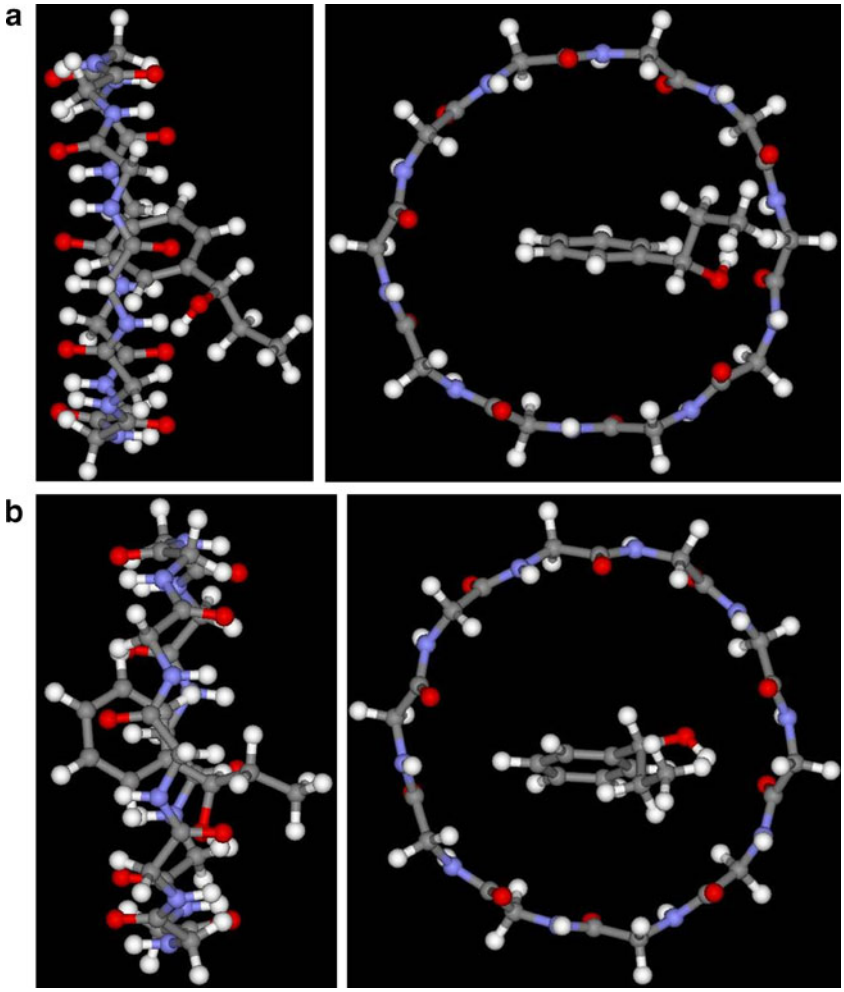

Fig. 3 Energy-minimized structure obtained by B3LYP/ 6-31+G(d,p) calculations for **CDP/E-PP**: (**a**) side view (left) and top view (right) for **CDP/S-PP** and (**b**) side view (left) and top view (right) for **CDP/R-PP**

All MD simulations were carried out using the AMBER9 [55] package with the AMBER force fields of parm99 [56, 57] and gaff [58]. The systems were explicitly solvated by using the TIP3P water potential inside a box large enough to ensure the solvent shell extended to 10 Å in all directions of each system studied. For the equilibration of the investigated systems, the following procedures were carried out. First, 22500 steps energy minimization were carried out to remove unfavorable contacts. Then the systems were heated over 100 ps from 0 to 300 K with a little restrains of 10 kcal mol^{-1} $Å^{-2}$. The equilibration time for each simulation was 500 ps (NPT) followed by 10 ns of data collection for trajectory analysis, that is, 5000 structures for each simulation were saved for further data analysis by uniformly sampling the trajectory.

With the help of a 10 ns long molecular dynamics, it is shown that the **CDP/E-PP** are stable in water environment. The detailed information of intermolecular hydrogen bonds interactions for the **CDP/E-PP** in the course of the simulations are listed in Table 3. The quantities and lifetimes of H-bonds reflect the ability of **CDP** to bind **E-PP**, respectively. These observations clearly show that the lifetimes and number of H-bonds for **CDP/S-PP** are longer and larger than those of **CDP/R-PP**. Specifically, the longest lifetime of H-bond for **CDP/S-PP** is up to 99.58% of the simulation times, while the longest

Table 2 The electron donors, electron acceptors and the corresponding $E^{(2)}$ energies, distances and angles obtained at the B3LYP/6-31+G(d,p) level of theory

	Donor	Acceptor	H…A (Å)	D…A (Å)	D–H…A (°)	$E^{(2)}$ (kJ mol^{-1})
CDP/S-PP	LP O1	BD*O11-H11	1.93	2.87	160.36	23.24
	LP O11	BD*C10-H10	2.48	3.40	140.94	8.41
CDP/R-PP	LP O5	BD*O11-H11	2.22	2.93	129.74	3.61

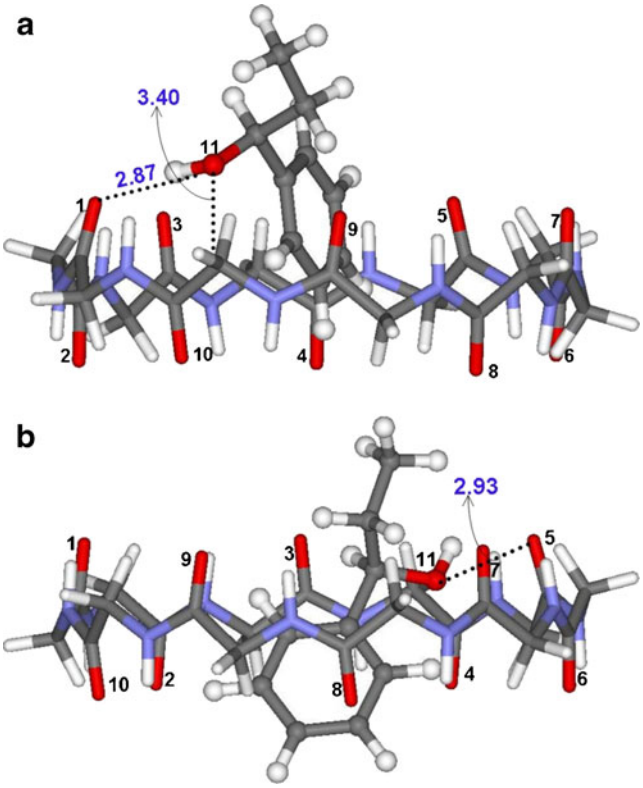

Fig. 4 Host–guest hydrogen bonds are presented by dotted lines: (**a**) **CDP**/**S-PP** and (**b**) **CDP**/**R-PP**. H in white, C in gray, N in blue, O in red

lifetime of H-bond for **CDP**/**R-PP** is only 44.06% of the simulation times. Compared to **R-PP**, **S-PP** exhibits the anticipated binding propensity to associate with **CDP**. The MD results indicate that the **CDP**/**S-PP** system is appreciably more stable than **CDP**/**R-PP**. Briefly, the MD results support the conclusions obtained by B3LYP/6-31+G(d,p).

Solvent effects

Complex phenomena take place in condensed phase. Thus, solvent plays a critical role in the intermolecular interactions that lead to the formation of inclusion complexes, especially in the case of polar compounds with hydrogen donor/acceptor groups. To consider the role of the solvent, the polarized continuum model (PCM) [59–61] has been employed to simulate the solvent effects as implemented within the solvent reaction field based on the optimized structures as listed in Table 1. As shown in Table 1, positive entropy changes (ΔS_{pcm}) in the two inclusion processes are 106.72 and 116.69 J mol^{-1} K^{-1} respectively, which are attributed to the releasing of water molecules in the cavity of **CDP**. Based on the discussions above, it can be concluded that entropy effects on the stability of the **CDP/E-PP** are favorable factors, that is, the formations of **CDP**/**E-PP** are entropy driven processes in aqueous solution.

Table 3 The intermolecular hydrogen bonds of **CDP**/**S-PP** and **CDP**/**R-PP** during molecular dynamics (MD) simulations

Complex	Donor	Acceptor	Lifetime (%)	Distance (Å)
CDP/S-PP	O1	O11-H11	99.58	2.82
	O11	C10-H10	95.82	3.65
CDP/R-PP	O5	O11-H11	44.06	2.99

Conclusions

In this work, **CDP/E-PP** have been investigated theoretically using the density functional theory (DFT) B3LYP method. Almost all possible locations of **E-PP** with **CDP** were taken into account to obtain the most stable conformation of **CDP/E-PP**. The optimized structures and the binding energy (BE) indicate that **CDP**/**S-PP** is more stable than **CDP**/**R-PP**. The conformational characteristics of **CDP/E-PP** show that the distinct differences for hydrogen bond interactions occur in the different **CDP**/**E-PP**. For **CDP**/**S-PP**, the better stabilization may be attributed to the formation of two hydrogen bonds between **CDP** and **E-PP**. For **CDP**/**R-PP**, only one hydrogen bond has been formed between **CDP** and **E-PP**, which might account for the stabilization of **CDP/E-PP**. The NBO analyses confirm the occurrence of these intermolecular hydrogen bonds: the NBO results show that there is one conventional hydrogen bond and one weak hydrogen bond in the **CDP/S-PP** inclusion complex while there is only one weak hydrogen bond in the **CDP/R-PP** inclusion complex. Briefly, these hydrogen bond interactions will contribute to the overall stability and structure of the inclusion complexes of **CDP** with **E-PP**. Furthermore, the MD simulation results are in agreement with the conclusions obtained by the B3LYP/6-31+G(d,p) method.

Additionally, the thermodynamic calculated results demonstrated that enthalpy changes (ΔH) are prominent in the inclusion processes. The enthalpy changes suggest that the formation of **CDP/E-PP** is an enthalpy driven process. Their obvious differences in binding energy and enthalpy change suggest that **CDP** could well distinguish **E-PP**. Take the solution effects into account, the entropy is still a favorable driving force for the formation of **CDP/E-PP**. The current studies provide a revealing insight into conformational characteristics and thermodynamics properties for **CDP/E-PP** at the molecular level. The observations in this work indicate that **CDP** is a desirable host molecule for chiral and molecular recognition.

Acknowledgments The work described in this paper was supported by the National Natural Science Foundation of China (No. 21001095) and China Postdoctoral Science Foundation (No. 20100480858).

References

1. Gellman SH (1997) Chem Rev 97:1231–1232
2. Breslow R, Dong SD (1998) Chem Rev 98:1997–2012
3. Lee WY, Park CH, Kim S (1993) J Am Chem Soc 115:1184–1185
4. Song LX, Wang HM, Yang Y (2007) Acta Chim Sinica 65:1593–1599
5. De Sousa FB, Denadai AML, Lula IS, Lopes JF, Dos Santos HF, De Almeida WB, Sinisterra RD (2008) Int J Pharm 353:160–169
6. Khedkar JK, Gobre W, Pinjari RV, Gejji SP (2010) J Phys Chem A 114:7725–7732
7. Maheshwari A, Sharma D (2010) J Incl Phenom Macro 68:453–459
8. Jug M, Mennini N, Melani F, Maestrelli F, Mura P (2010) Chem Phys Lett 500:347–354
9. Wen XH, Liu ZY, Zhu TQ (2005) Chem Phys Lett 405:114–117
10. Zoppi A, Quevedo MA, Delrivo A, Longhi MR (2010) J Pharm Sci 99:3166–3176
11. Dos Santos HF, Duarte HA, Sinisterra RD, De Melo Mattos SV, De Oliveira LFC, De Almeida WB (2000) Chem Phys Lett 319:569–575
12. Snor W, Liedl E, Weiss Greiler P, Virnstein H, Wolschann P (2009) Int J Pharm 381:146–152
13. Barbiric DJ, Castro EA, de Rossi RH (2000) J Mol Struct THEOCHEM 532:171–181
14. Seridi L, Boufelfel A (2011) J Mol Liq 158:151–158
15. Chankvetadze B (1997) J Chromatogr A 792:269–295
16. Fanali S (2000) J Chromatogr A 875:89–122
17. Armstrong DW, Nair UB (1997) Electrophoresis 18:2331–2342
18. Ward TJ, Oswald TM (1997) J Chromatogr A 792:309–325
19. Haginaka J (2000) J Chromatogr A 875:235–254
20. Otsuka K, Terabe S (2000) J Chromatogr A 875:163–178
21. Castillo N, Boyd RJ (2005) Chem Phys Lett 416:70–74
22. Kim H, Jeong K, Lee S, Jung S (2002) J Comput Aided Mol Des 16:601–610
23. Stella VJ, Rao VM, Zannou EA, Zia V (1999) Adv Drug Deliv Rev 36:3–16
24. Schneiderman E, Stalcup AM (2000) J Chromatogr B 745:83–102
25. Coleman AW (1998) Kluwer Academic Publishers, p 103
26. Kobayashi J, Tsuda M, Nakamura T, Mikami Y, Shigemori H (1993) Tetrahedron 49:2391–2402
27. Gulavita NK, Gunasekera SP, Pomponi SA, Robinson EV (1992) J Org Chem 57:1767–1772
28. Ferrante F, La Manna G (2007) J Comput Chem 28:2085–2090
29. Lewis JP, Pawley NH, Sankey OF (1997) J Phys Chem B 101:10576–10583
30. Maier NM, Schefzick S, Lombardo GM, Feliz M, Rissanen K, Lindner W, Lipkowitz KB (2002) J Am Chem Soc 124:8611–8629
31. Kim KS, Cui C, Cho SJ (1998) J Phys Chem B 102:461–463
32. Zhu YY, Tang MS, Shi XY, Zhao YF (2007) Int J Quantum Chem 107:745–753
33. Teranishi M, Okamoto H, Takeda K, Nomura K, Nakano A, Kalia RK, Vashishta P, Shimojo F (2009) J Phys Chem B 113:1473–1484
34. Chen GJ, Su S, Liu RZ (2002) J Phys Chem B 106:1570–1575
35. Tan HW, Qu WW, Chen GJ, Liu RZ (2003) Chem Phys Lett 369:556–562
36. Khattabi S, Cherrak DE, Mihlbachler K, Guiochon G (2000) J Chromatogr A 893:307–319
37. Okamoto H, Nakanishi T, Nagai Y, Kasahara M, Takeda K (2003) J Am Chem Soc 125:2756–2769
38. Yan CL, Xiu ZL, Li XH, Hao C (2007) J Mol Graph Model 26:420–428
39. Liu L, Guo QX (2004) J Incl Phenom Macrocycl Chem 50:95–103
40. Becke AD (1993) J Chem Phys 98:5648–5652
41. Lee C, Yang W, Parr RG (1988) Phys Rev B 37:785–789
42. Ohashi M, Kasatani K, Shinohara H, Sato H (1990) J Am Chem Soc 112:5824–5830
43. Glendening ED, Reed AE, Carpenter JE, Weinhold F, NBO Version 03.01, included in the GAUSSIAN 03 package of programs
44. Zhu YY, Chen ZF, Guo ZJ, Wang Y, Chen GG (2009) J Mol Model 15:469–479
45. van Duijneveldt FB, van Duijneveldt-van de Rijdt JGCM, van Lenthe JH (1994) Chem Rev 94:1873–1885
46. Frisch MJ, Trucks GW, Schlegel HB, Scuseria GE, Robb MA, Cheeseman JR, Montgomery JA, Vreven JT, Kudin KN, Burant JC, Millam JM, Iyengar SS, Tomasi J, Barone V, Mennucci B, Cossi M, Scalmani G, Rega N, Petersson GA, Nakatsuji H, HadaM EM, Toyota K, Fukuda R, Hasegawa J, Ishida M, Nakajima T, Honda Y, Kitao O, Nakai H, KleneM Li X, Knox JE, Hratchian HP, Cross JB, Bakken V, Adamo C, Jaramillo J, Gomperts R, Stratmann RE, Yazyev O, Austin AJ, Cammi R, Pomelli C, Ochterski JW, Ayala PY, Morokuma K, Voth GA, Salvador P, Dannenberg JJ, ZakrzewskiVG DS, Daniels AD, Strain MC, Farkas O, Malick DK, Rabuck AD, Raghavachari K, Foresman JB, Ortiz JV, Cui Q, Baboul AG, Clifford S, Cioslowski J, Stefanov BB, Liu G, Liashenko A, Piskorz P, Komaromi I, Martin RL, Fox DJ, Keith T, Al-Laham MA, Peng CY, Nanayakkara A, Challacombe M, Gill PMW, Johnson B, Chen W, Wong MW, Gonzalez C, Pople JA (2004) Gaussian 03. Gaussian Inc, Wallingford, CT
47. Rekharsky MV, Inoue YI (1998) Chem Rev 98:1875–1917
48. Starikov EB, Saenger W, Steiner Th (1998) Carbohydr Res 307:343–346
49. Uccello Barretta G, Balzano F, Sicoli G, Paolino D, Guccione S (2004) Bioorg Med Chem 12:447–458
50. Desiraju GR (1996) Chem Res 29:441–449
51. Steiner T (1997) Chem Commun 727-734
52. Yu YM, Christophe C, Cai WS, Shao XG (2006) J Phys Chem B 110:6372–6378
53. Cai WS, Sun TT, Liu P, Christophe C, Shao XG (2009) J Phys Chem B 113:7836–7843
54. Morris GM, Goodse DS, Halliday RS, Huey R, Hart WE, Belew RK, Olson AJ (1998) J Comput Chem 19:1639–1662
55. Case DA, Darden TA, Cheatham TE, Simmerling CL, Wang J, Duke RE, Luo R, Merz KM, Pearlman DA, Crowley M, Walker RC, Zhang W, Wang B, Hayik S, Roitberg A, Seabra G, Wong KF, Paesani F, Wu X, Brozell S, Tsui V, Gohlke H, Yang L, Tan C, Mongan J, Hornak V, Cui G, Beroza P, Mathews DH, Schafmeister C, Ross WS, Kollman PA (2006) AMBER 9. University of California, San Francisco
56. Duan Y, Wu C, Chowdhury S, Lee MC, Xiong G, Zhang W, Yang R, Cieplak P, Luo R, Lee T (2003) J Comput Chem 24:1999–2012
57. Lee MC, Duan Y (2004) Proteins 55:620–634
58. Wang J, Wolf RM, Caldwell JW, Kollamn PA, Case DA (2004) J Comput Chem 25:1157–1174
59. Rehbein J, Hiersemann M (2009) J Org Chem 74:4336–4342
60. Peles DN, Thoburn JD (2008) J Org Chem 73:3135–3144
61. Takano Y, Houk KN (2005) J Chem Theor Comput 1:70–77